Available online at www.sciencedirect.com
ScienceDirect
Journal of Catalysis 251 (2007) 103–112
JOURNAL OF CATALYSIS
www.elsevier.com/locate/jcat

A comparative study of substituted perovskite-type solids of oxidic $La_{1-x}Sr_xFeO_{3\pm\delta}$ and chlorinated $La_{1-x}Sr_xFeO_{3\pm\delta}Cl_\sigma$ form: Catalytic performance for CH_4 oxidation by O_2 or N_2O

A.A. Leontiou [a,*], A.K. Ladavos [b], A.E. Giannakas [a], T.V. Bakas [c], P.J. Pomonis [a]

[a] *Department of Chemistry, University of Ioannina, Ioannina 45 110, Greece*
[b] *School of Natural Resources and Enterprise Management, University of Ioannina, Agrinio 30 100, Greece*
[c] *Department of Physics, University of Ioannina, Ioannina 45 110, Greece*

Received 23 April 2007; revised 4 July 2007; accepted 8 July 2007

Available online 22 August 2007

Abstract

A comparative study between two groups of substituted perovskite-type solids, one oxidic and another chlorinated with general formulas $La_{1-x}Sr_xFeO_{3\pm\delta}$ and $La_{1-x}Sr_xFeO_{3\pm\delta}Cl_\sigma$ ($x = 0.0, 0.4, 0.6$ and 0.8), was carried out for the oxidation of CH_4 by O_2 and N_2O. For stoichiometric feeding compositions $CH_4{:}O_2 = 1{:}2$ and $CH_4{:}N_2O = 1{:}4$, the catalysts were active in the temperature range 400–760 °C. The oxidic solids were more active than the chlorinated ones. Catalysts of both groups, containing Sr, exhibited a drop in activity for the above reactions, related to an increased amount of desorbed oxygen from the solids. The amount of desorbed oxygen is linearly correlated with the Fe^{4+} content in the solid. The lower activity of the chlorinated samples can be attributed to a poisoning effect by chlorine, the quantity of which was estimated using proper deactivation kinetics.

Keywords: Perovskite; Oxidic; Chlorinated; Methane oxidation

1. Introduction

Perovskite-type oxides have been attracting great attention in environmental-related catalytic fields. Catalytic combustion over perovskite-type solids, noble metal-containing and/or -supported perovskites has been proposed as a method for reducing thermal NO_x emissions due to the possibility of carrying out the reaction at lower temperatures compared with conventional flame combustion [1–6]. Interest lies in the study of substitution of trivalent cations in the site A by divalent ones with similar ionic radii, which alters the oxidation state of B cations, giving rise to mixed valence states [7–10]. The creation of nonstable valence states and the establishment of metal or oxygen nonstoichiometry have drawn much attention for various physicochemical processes, including catalysis, photocatalysis, conductivity, and others [11,12]. Another distinct possibility for such solids is to study their halogenated form, which can be represented by the formula $ABO_{3-\sigma}X_\sigma$, where X represents Cl or F. The literature on this subject is rather limited. Generally, the incorporation of halide ions with ionic radii similar to that of O^{2-} can be expected to alter the oxygen vacancy density of such solids.

Characterization of the perovskite-type chloro-oxide $SrFeO_{3-\delta}Cl_\sigma$ by Dai et al. [13] showed that the partial substitution of chloride ions for oxygen ions did not induce any obvious change in crystal structure. However, the Fe^{4+}/Fe^{3+} ratio appeared to be increased compared with that of the nonhalogenated solids. Fluorination was found to decrease the stability of the original $La_{1-x}Sr_xMnO_3$ perovskite structure [14]; that is, the lattice parameters and unit cell volumes decreased with F doping, and $La_{1-x}Sr_xMnO_{3-2x+\delta}F_{2x}$ samples suffered a structural transition from rhombohedral to orthorhombic at $x = 0.30$.

As suggested by Conway et al. [15], the presence of Cl^- ions in the catalyst might improve the catalytic activity by pro-

* Corresponding author. Fax: +32641039579.
E-mail address: aleontiu@cc.uoi.gr (A.A. Leontiou).

0021-9517/$ – see front matter
doi:10.1016/j.jcat.2007.07.012

tecting the active sites from CO_2 poisoning. Lee and Ng used $YBa_2Cu_2O_{6+x-z}F_z$ compounds as catalysts for the partial combustion of methane and found that the incorporation of F^- ions enhanced the tendency for the partial oxidation reaction [16].

In catalytic experiments for the oxidative dehydrogenation of ethane (ODE), the catalyst $SrFeO_{3-0.382}Cl_{0.443}$ was much superior to $SrFeO_{3-0.190}$, reaching an ethane selectivity of ca. 70% at 680 °C [13]. These same authors reported [17] that halide-modified $La_{1-x}Sr_xFeO_{3-\delta}X_\sigma$ performed much better than $La_{1-x}Sr_xFeO_{3-\delta}$ catalysts for the ODE reaction and that this good performance was related to the nature of the defect induced by the introduction of halide ions into the perovskites. Although numerous authors have reported comparative studies of the oxidative coupling of methane over irreducible [18] and reducible [19] oxides using both oxidants, reports on the oxidation of methane by N_2O on perovskite-type solids are limited.

N_2O is believed to be implicated in the destruction of ozone layer and is acknowledged as a relatively strong greenhouse gas. It contributes to global warming much more than the anthropogenic greenhouse gas methane [20]. Large quantities of nitrous oxide are produced in combustion, in the production of adipic and nitric oxides and fertilizers, and in mobile and stationary NO_x-reduction processes [21]. Thus, it is of interest to examine the oxidation of methane using N_2O as an oxidant in an attempt to reduce N_2O emissions.

The present work represents a systematic attempt to characterize and compare a group of oxidic-substituted perovskite solids, $La_{1-x}Sr_xFeO_{3\pm\delta}$, with the corresponding chlorinated ones, $La_{1-x}Sr_xFeO_{3\pm\delta}Cl_\sigma$ ($x = 0.0$, 0.4, 0.6, and 0.8), for the deep oxidation of methane. Along with the conventional method using oxygen for oxidation, nitrous oxide also was used as an oxidant. The structure of the solids and the valence state of Fe ions were studied using XRD and Mössbauer spectroscopy, respectively. The oxygen nonstoichiometric composition of the samples was checked by thermogravimetric O_2/TPD experiments. The chlorine content of the samples was checked by SEM-EDS analysis. The purpose of the study was to correlate quantitatively the catalytic activity with various physicochemical characteristics, as well as to scrutinize the role of chlorine on the catalytic performance of the examined solids.

2. Experimental

2.1. Sample preparation and characterization

The solids of the two groups with nominal formulas $La_{1-x}Sr_xFeO_{3\pm\delta}$ and $La_{1-x}Sr_xFeO_{3\pm\delta}Cl_\sigma$, with $x = 0.0$, 0.4, 0.6, and 0.8, were prepared according to the ceramic method as described below. The samples $LaFeO_{3\pm\delta}$, $La_{0.6}Sr_{0.4}FeO_{3\pm\delta}$, $La_{0.4}Sr_{0.6}FeO_{3\pm\delta}$, and $La_{0.2}Sr_{0.8}FeO_{3\pm\delta}$ are members of the group $La_{1-x}Sr_xFeO_{3\pm\delta}$, for which the preparation method has been described previously [22]. Calculated amounts (Table 1) of $La(NO_3)_3{\cdot}6H_2O$ (Fluka), $Sr(NO_3)_2$ (Ferak), and $Fe(NO_3)_3{\cdot}9H_2O$ (Merck) for the series $La_{1-x}Sr_xFeO_{3\pm\delta}$ and $La(Cl)_3{\cdot}7H_2O$ (Merck), $SrCl_2{\cdot}6H_2O$ (Aldrich), and $Fe(NO_3)_3{\cdot}9H_2O$ (Merck) for the series $La_{1-x}Sr_xFeO_{3\pm\delta}Cl_\sigma$ were mixed and heated to 400 °C at a rate of 3 °C/min for complete nitrate decomposition. When no NO_x fumes were visible, the samples were heated for another 4 h at 900 °C at atmospheric conditions. After cooling and grinding in an agate mortar, they were then heated for another 4 h at 1000 °C. The properties of the solids thus obtained after cooling are given in Table 2.

The specific surface area of the prepared materials was checked by N_2 adsorption (BET) at 77 K using a single-point Carlo-Erba Sorpty 1750 apparatus. Before measurement, all samples were degassed at 250 °C for 4 h at 4 mbar. The results are given in Table 2.

The crystal structure of the tested catalysts was determined by XRD diffraction analysis carried out using a BRÜKER D8 ADVANCE system using Cu$K\alpha$ radiation ($\lambda = 1.5418$ Å). The samples were placed in quartz sample holders, and step scans were obtained over the range of 2θ angles of 10–80° in steps of 0.02° (2θ). The XRD patterns shown in Fig. 1 were assigned by comparison with the Joint Committee on Powder Diffraction Standards database.

^{57}Fe Mössbauer spectra were obtained for all samples at room temperature. A constant acceleration spectrometer was used to move a ^{57}Co (Rh) source kept at room temperature. The spectrometer was calibrated with α-Fe at room temperature; isomer shift values [23] are given relative to this. The corresponding spectra for the oxidic group of solids and the spectra for the chlorinated samples are shown in Fig. 2.

O_2 temperature-programmed desorption (TPD) experiments for the prepared solids were conducted using a Netzch STA 449C thermal analyzer. A detailed description of the experimental procedure has been published previously [22]. Briefly, each sample (~70 mg) was placed in an alumina crucible, and Al_2O_3, which undergoes no thermal change in the temperature range of the experiment, was placed in an identical crucible as a reference sample. The temperature of the samples was measured by thermocouples of Pt and of Pt/10% Rh. The sample was first pretreated in a He stream (20 ml min^{-1}) from ambient temperature up to 700 °C so as to allow desorption of any gases present on the catalyst surface. After this, it was progressively cooled to 550 °C in the same atmosphere and then kept under O_2 flow (20 ml min^{-1}) for 1 h. After cooling to 70 °C, a gas flow of He (10 ml min^{-1}) was passed through the sample to wash out any oxygen molecules not chemisorbed. The temperature was then raised to 900 °C at a rate of 10 °C min^{-1}. The parameters recorded simultaneously were temperature (T) and change in weight (by thermogravimetric [TG] analysis).

Analysis of the chlorinated solids was carried in a JEOL JSM 5600 scanning electron microscopy (SEM) system. This analysis was performed in conjunction with energy-dispersive X-ray spectroscopy (EDS) to characterize the elemental composition of the analyzed sample. The values of Cl content (% w/w) were calculated for each sample and are given in Table 2. These values are the mean values of 10 measurements at various areas of the examined sample on the sample holder using small factors of magnification in the scanning electron microscope. The estimated values are reliable for all samples except the unsubstituted sample ($x = 0$), for which the value of chlorine is equal to the detective limit of the technique.

Table 1
Calculated amounts of salts used for the preparation

Sample	$La(NO_3)_3{\cdot}6H_2O$ (g)	$Sr(NO_3)_2$ (g)	$Fe(NO_3)_3{\cdot}9H_2O$ (g)
$LaFeO_{3\pm\delta}$	8.9189	0.0000	8.3213
$La_{0.6}Sr_{0.4}FeO_{3\pm\delta}$	5.8454	1.9000	9.0894
$La_{0.4}Sr_{0.6}FeO_{3\pm\delta}$	4.0855	2.9880	9.5292
$La_{0.2}Sr_{0.8}FeO_{3\pm\delta}$	2.1466	4.1865	10.0137
Sample	$LaCl_3{\cdot}7H_2O$ (g)	$SrCl_2{\cdot}6H_2O$ (g)	$Fe(NO_3)_3{\cdot}9H_2O$ (g)
$LaFeO_{3\pm\delta}Cl_\sigma$	5.7116	0.0000	6.2133
$La_{0.6}Sr_{0.4}FeO_{3\pm\delta}Cl_\sigma$	3.8364	1.8361	6.9556
$La_{0.4}Sr_{0.6}FeO_{3\pm\delta}Cl_\sigma$	2.7201	2.9292	7.3975
$La_{0.2}Sr_{0.8}FeO_{3\pm\delta}Cl_\sigma$	1.4523	4.1705	7.8993

Table 2
Prepared solids, detected crystal phases (XRD), amount of oxygen desorbed in the O_2/TPD experiments and % weight Cl content estimated by EDS analysis

Nominal composition	Crystal phases (XRD)	Specific surface area ($m^2\ g^{-1}$)	TPD O_2 (μmol/g)	% Cl content
	$La_{1-x}Sr_xFeO_{3\pm\delta}$ samples			
$LaFeO_{3\pm\delta}$	$LaFeO_3$, La_2O_3, Fe_2O_3	3.1	0.0	–
$La_{0.6}Sr_{0.4}FeO_{3\pm\delta}$	$La_{0.6}Sr_{0.4}FeO_3$, $SrFeO_3$, La_2O_3,[a] Fe_2O_3[a]	3.5	314.5	–
$La_{0.4}Sr_{0.6}FeO_{3\pm\delta}$	$La_{0.4}Sr_{0.6}FeO_3$, $SrFeO_3$, La_2O_3,[a] Fe_2O_3[a]	3.1	402.3	–
$La_{0.2}Sr_{0.8}FeO_{3\pm\delta}$	$La_{0.3}Sr_{0.7}FeO_3$, $SrFeO_3$	3.4	586.8	–
	$La_{1-x}Sr_xFeO_{3\pm\delta}Cl_\sigma$ samples			
$LaFeO_{3\pm\delta}Cl_\sigma$	$LaFeO_3$	2.8	40.6	0.5
$La_{0.6}Sr_{0.4}FeO_{3\pm\delta}Cl_\sigma$	$La_{0.6}Sr_{0.4}FeO_3$	2.8	78.6	2.1
$La_{0.4}Sr_{0.6}FeO_{3\pm\delta}Cl_\sigma$	$La_{0.4}Sr_{0.6}FeO_3$, $SrFe_{12}O_{19}$	2.6	121.9	1.5
$La_{0.2}Sr_{0.8}FeO_{3\pm\delta}Cl_\sigma$	$La_{0.3}Sr_{0.7}FeO_3$, $Sr_3Fe_2O_5Cl_2$, $SrFe_{12}O_{19}$	3.1	187.5	6.4

[a] Traces.

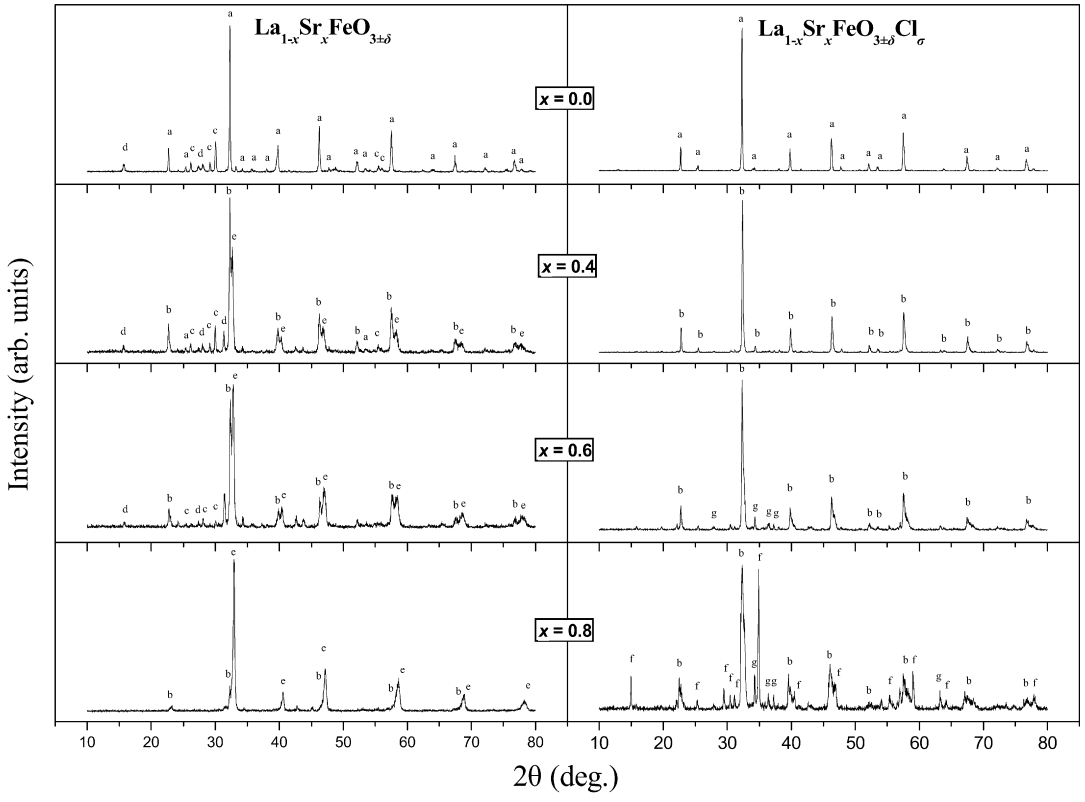

Fig. 1. X-ray diffraction patterns of the samples $La_{1-x}Sr_xFeO_{3\pm\delta}$ (left) and $La_{1-x}Sr_xFeO_{3\pm\delta}Cl_\sigma$ group (right) calcined at 1000 °C. The lines correspond to the following crystal phases (all data from the JCPDS Data Bank): a—$LaFeO_3$, b—$La_{0.6}Sr_{0.4}FeO_3$, c—La_2O_3, d—Fe_2O_3, e—$SrFeO_3$, f—$La_{0.4}Sr_{0.6}FeO_3$, g—$La_{0.3}Sr_{0.7}FeO_3$, h—$SrFe_{12}O_{19}$, and k—$Sr_3Fe_2O_5Cl_2$.

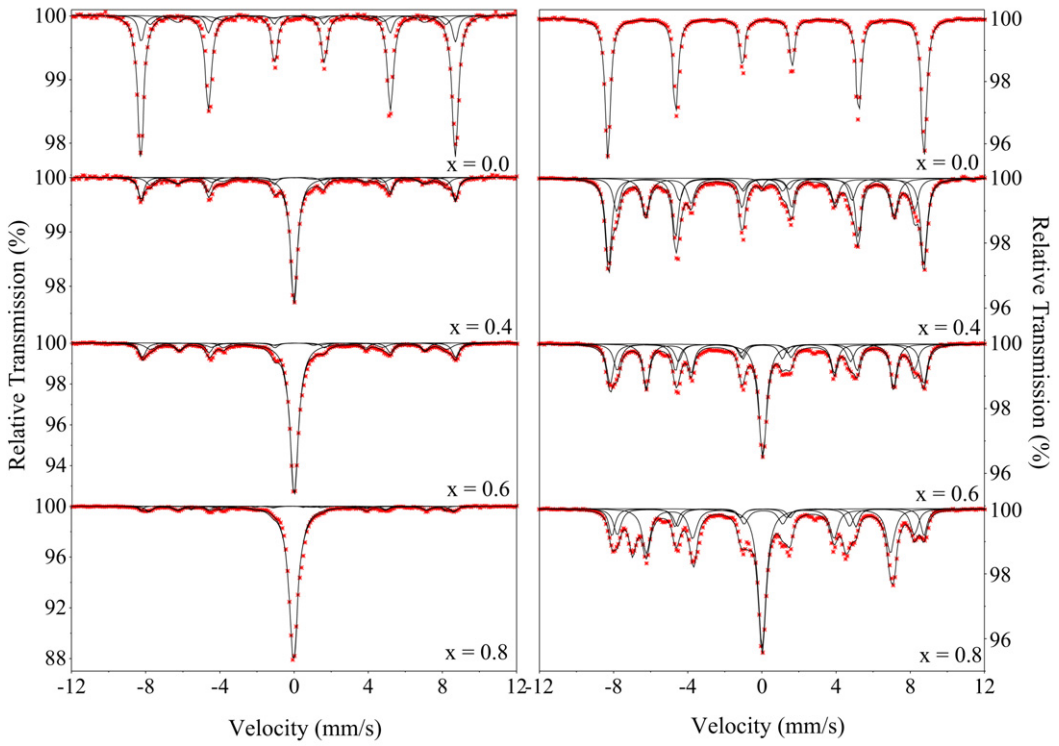

Fig. 2. Mössbauer spectra at RT for the oxidic $La_{1-x}Sr_xFeO_{3\pm\delta}$ (left) and chlorinated $La_{1-x}Sr_xFeO_{3\pm\delta}Cl_\sigma$ solids (right). Crosses denote experimental data. The results of the least squares fit as well as its spectral components are drawn by solid lines.

2.2. Catalytic activity tests

The catalytic oxidation of methane was carried out in a fixed-bed bench-scale tubular reactor at atmospheric pressure. The reactor was heated externally using a tubular furnace, regulated by a JUMO iTRON 16 controller, via a thermocouple placed in the center of the catalyst bed, within ±1 °C. The product analysis was accomplished using an on-line Shimadzu 15A gas chromatograph equipped with a thermal conductivity detector with helium as the carrier gas and connected to a Chromatopak C-R6A integrator system. The carrier gas flow was kept at 30 ml min^{-1}, and the product line from the exit of the reactor to the injector port was kept at 100 °C, to avoid condensation of the water produced. A 10-port valve enabled sampling of 1 ml of reactant or product for analysis using two columns, a Porapaq Q and a Molecular Sieve 13X.

Two sets of experiments were carried out differing in the kind of gas used as an oxidant: O_2 in one case (I) and N_2O in the other (II). A 250-mg catalyst sample was placed on quartz wool in the middle of the reactor, and a cleaning procedure involving flowing helium (30 ml min^{-1} at 600 °C for 30 min was applied. After cooling to 400 °C, the reaction mixture was fed by mass flow controllers (MKS type 247) in either a total flow of 115 ml min^{-1} with CH_4:O_2:He = 4.35:8.7:86.95 vol% (case I) or a total flow of 120 ml min^{-1} with CH_4:N_2O:He = 5:20:75 vol% (case II). In both cases, the flow values and the corresponding ratios were set equal to the stoichiometry of total methane oxidation. The catalysts were tested at intervals of 40 °C up to 800 °C, and the detected and quantitatively calculated products were CO_2 in case I and N_2, CO_2 in case II. The detected water was not included in any quantitative calculations.

3. Results and discussion

3.1. XRD study

XRD images of the tested samples are shown in Fig. 1, and the results are summarized in Table 2. In the parent oxidic sample, $LaFeO_{3\pm\delta}$ ($x = 0.0$), the major $LaFeO_3$ perovskite phase and two other phases of Fe_2O_3 and La_2O_3 were detected. Then, with gradual substitution of La^{3+} by Sr^{2+} ($x = 0.4$, 0.6, 0.8), along with the corresponding perovskite crystal phase, a well-defined crystal phase $SrFeO_3$ also was apparent. For the final sample ($x = 0.8$), the $SrFeO_3$ crystal phase predominated.

The addition of Cl in the oxidic samples resulted in the production of pure perovskite crystal phases in the low Sr-content samples ($x = 0.0$ and 0.4) (Fig. 1). For samples with higher Sr content ($x = 0.6$, 0.8), the presence of even higher amounts of Cl resulted in the formation of other phases such as $SrFe_{12}O_{19}$ and $Sr_3Fe_2O_7$. In the final sample ($x = 0.8$), a chlorinated perovskite $Sr_3Fe_2O_5Cl_2$ was formed. In conclusion, the addition of Cl stabilized the perovskite phase for the low Sr-content ($x \leqslant 0.6$) samples but destabilized the perovskite phase for the high Sr-content ($x = 0.8$) samples.

3.2. Mössbauer spectra

The spectra corresponding to the first samples of both series ($x = 0.0$) were composed of at least one superimposed six-line

pattern. The hyperfine parameters deduced after least squares computer minimization show that these magnetic components corresponded to Fe^{3+}. For the rest of the samples ($x \geqslant 0.4$), a singlet near zero velocity appeared, corresponding to Fe^{4+}.

Table 3 summarizes the corresponding hyperfine parameters deduced after analysis of the Mössbauer spectra obtained at room temperature, the hyperfine magnetic field detected from the 57-Fe nucleus (H_{eff}, T), quadrupole splitting (ΔE_q, $mm\,s^{-1}$), and the isomer shift value relative to Fe metal (δ_{Fe}, $mm\,s^{-1}$), as well as the percentage (%) contribution of Fe^{3+} in various crystal phases or Fe^{4+} in the $SrFeO_3$ crystal phase to the total area of the spectrum. The area under each crystal component (singlet, doublet, or sextet) used for the analysis is proportional to the amount of the crystal phase in the sample.

Assuming that all crystal phases have the same recoil-free fraction, the experimental data were analyzed by a least squares computer minimization procedure, using a sum of Lorentzian spectral components characterizing different iron phases [24]. We see that the percentage (%) of Fe^{4+} in the solids increased with increasing degree of substitution x, reaching a value of 81% in the solid with nominal composition $La_{0.2}Sr_{0.8}FeO_{3\pm\delta}$ of the first group, compared with only 22% for the corresponding sample $La_{0.2}Sr_{0.8}FeO_{3\pm\delta}Cl_\sigma$ of the second chlorinated group.

For the samples with $x = 0.0$, only Fe^{3+} was detected in perovskite phase $LaFeO_3$, whereas in those with higher degrees of substitution ($x = 0.4, 0.6, 0.8$), Fe^{3+} also was detected in various Fe-containing crystal phases. The contribution of the Fe^{4+} spectral component increased considerably with increasing x, reaching higher values in oxidic samples, as already mentioned. The chlorinated samples always contained more Fe^{3+} and less Fe^{4+} than the corresponding oxidic samples.

3.3. Thermogravimetric O_2/TPD analysis

Fig. 3 shows the change in sample weight (determined by TG analysis) versus temperature during the last step of the procedure—heating the sample to 900 °C at a rate of 10 °C min^{-1}—isolated from the other steps. Figs. 3a and 3b compare the recorded TG curves versus temperature for the oxidic $La_{1-x}Sr_xFeO_{3\pm\delta}$ and the chlorinated $La_{1-x}Sr_xFeO_{3\pm\delta}Cl_\sigma$ samples. These curves demonstrate that the sample weight decreases with increasing temperature. The observed weight loss during the last calcination step of the procedure corresponds to oxygen desorption. The arrows and the line that corresponds to a 0.2% loss aid a quantitative comparison of the weight loss in the two groups. The results correspond to the specific sample mass of about 70 mg used for the TPD experiments. Figs. 3c and 3d show the DTG curves arising from differentiation of the TG curves. The corresponding peaks of these curves show the temperature region in which the maximum desorption rate was observed.

The weight loss during the last calcination step of the O_2/TPD experiments at 70–900 °C corresponds to the amount of oxygen desorbed from the samples. This can be easily calculated from the TG results given in Figs. 3a and 3b. The estimated values of desorbed oxygen, in μmol per gram of sample, are given in Table 2. Both groups of solids are characterized

Table 3
The percentage of the identified crystal phases containing iron in the oxidic and in the chlorinated samples and Mössbauer hyperfine parameters at RT

Solid (nominal composition)	Phases containing Fe^{3+}												Phases containing Fe^{4+}			
	Fe^{3+} in La–Sr–Fe–O phase				Fe^{3+} in Fe_2O_3 phase				Fe^{3+} in $SrFeO_{3-x}$ phase				Fe^{4+} in $SrFeO_{3-x}$ phase			
	H_{eff} (T)	δ_{Fe} ($mm\,s^{-1}$)	ΔE_q ($mm\,s^{-1}$)	Area (%)	H_{eff} (T)	δ_{Fe} ($mm\,s^{-1}$)	ΔE_q ($mm\,s^{-1}$)	Area (%)	H_{eff} (T)	δ_{Fe} ($mm\,s^{-1}$)	ΔE_q ($mm\,s^{-1}$)	Area (%)	H_{eff} (T)	δ_{Fe} ($mm\,s^{-1}$)	ΔE_q ($mm\,s^{-1}$)	Area (%)
$La_{1-x}Sr_xFeO_{3\pm\delta}$ samples																
$LaFeO_{3\pm\delta}$	52.7	0.37	−0.08	100	–	–	–	–	–	–	–	–	–	–	–	–
$La_{0.6}Sr_{0.4}FeO_{3\pm\delta}$	52.6	0.37	−0.06	26	49.6	0.32	0.03	14	41.4	0.34	0.31	14	0.0	0.11	0.00	46
$La_{0.4}Sr_{0.6}FeO_{3\pm\delta}$	52.5	0.37	−0.04	18	49.6	0.29	0.09	13	41.2	0.32	0.41	10	0.0	0.10	0.00	59
$La_{0.2}Sr_{0.8}FeO_{3\pm\delta}$	52.2	0.38	−0.03	3	50.3	0.30	0.16	10	41.6	0.34	0.44	6	0.0	0.09	0.00	81
$La_{1-x}Sr_xFeO_{3\pm\delta}Cl_\sigma$ samples																
$LaFeO_{3\pm\delta}Cl_\sigma$	53.0	0.37	−0.07	100	–	–	–	–	–	–	–	–	–	–	–	–
$La_{0.6}Sr_{0.4}FeO_{3\pm\delta}Cl_\sigma$	52.9	0.37	−0.04	49	50.0	0.32	−0.01	23	41.6	0.36	0.37	26	0.0	0.12	0.00	1
$La_{0.4}Sr_{0.6}FeO_{3\pm\delta}Cl_\sigma$	52.6	0.37	0.03	28	49.8	0.29	0.07	21	41.4	0.36	0.39	29	0.0	0.16	0.00	22
$La_{0.2}Sr_{0.8}FeO_{3\pm\delta}Cl_\sigma$	52.3	0.38	0.14	13	49.8	0.27	0.12	16	40.9	0.33	0.28	28	0.0	0.13	0.00	22

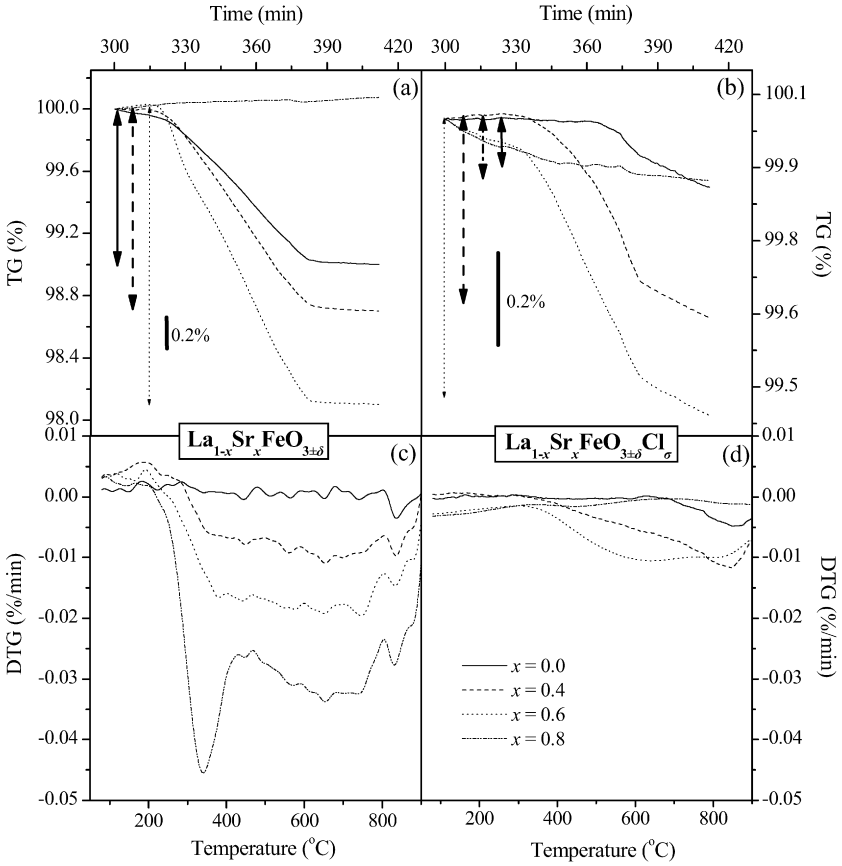

Fig. 3. Temperature-programmed desorption profiles of oxygen from the oxidic $La_{1-x}Sr_xFeO_{3\pm\delta}$ (left) and chlorinated $La_{1-x}Sr_xFeO_{3\pm\delta}Cl_\sigma$ (right) solids observed during the last step of the experiment. The corresponding DTG signals are shown in the lower part.

by an increasing amount of desorbed oxygen with increasing degree of substitution x. However, these values are noticeably higher for the oxidic group $La_{1-x}Sr_xFeO_{3\pm\delta}$ compared with the chlorinated group $La_{1-x}Sr_xFeO_{3\pm\delta}Cl_\sigma$. It must be stressed that the oxygen desorption occurred mainly at 350–400 °C in $La_{1-x}Sr_xFeO_{3\pm\delta}$ (Fig. 3c), compared with 600–800 °C in $La_{1-x}Sr_xFeO_{3\pm\delta}Cl_\sigma$ (Fig. 3d).

A graph presenting the general trend of oxygen desorption with respect to % Fe^{4+} for both groups is shown in Fig. 4. The gradual substitution of La^{3+} by Sr^{2+} resulted in the transformation of Fe^{3+} to Fe^{4+} in the oxidic perovskites. The addition of Cl in the solids decreased the percentage of Fe^{4+}. The reducing effect of Cl^- in the perovskite structure (i.e., the dramatic decrease in Fe^{4+} content), although strange at a first glance, can be explained according to the following reasoning: Substitution of the divalent O^{2-} anions by the monovalent Cl^- ones creates the need for *less* positive charges per unit cell to keep the electrostatic charges balanced. For example, in a chlorinated solid $LaFeO_{3-\sigma}Cl_\sigma$, for $\sigma = 1$, the typical valence of Fe should be +2.5, if O and La retain their typical valences of −2 and +3, respectively. This is in contrast to the oxidic solid $LaFeO_3$ ($\sigma = 0$), in which Fe appears with a typical valence of +3. In a similar fashion, under ideal conditions, 50% substitution of La^{3+} by Sr_{2+} would lead to a solid $La^{+3}_{0.5}Sr^{2+}_{0.5}Fe^{+3}_{0.5}Fe^{+4}_{0.5}O^{-2}_3$. But if in this latter material, 10% of the lattice oxygen O^{-2} were substituted by Cl^{-1}, then the theoretical/ideal solid should be $La^{+3}_{0.5}Sr^{+2}_{0.5}Fe^{+3}_{0.8}Fe^{+4}_{0.2}O^{-2}_{2.7}Cl^{-1}_{0.3}$.

As for the stabilization of the chlorinated perovskite structures compared with the oxidic structure, we suggest that this is due to the well-known "tolerance factor," t, of the perovskite structure [25]. This geometric parameter is given by the formula

$$t = \frac{r_A + r_X}{1.41(r_B + r_X)}, \tag{1}$$

where r_A, r_B, and r_X are the radii of the A and B cations and the X anion. Then, using the values of standard ionic radii [26], for various perovskites we obtain the following values:

for $LaFeO_3$: $t = 0.84$; (2)

for $LaFeCl_6$: $t = 0.82$; (3)

for $SrFeO_3$: $t = 0.95$; (4)

for $SrFeCl_6$: $t = 0.90$; (5)

for $La_{0.5}Sr_{0.5}Fe^{+3}_{0.5}Fe^{+4}_{0.5}O_3$: $t = 0.90$; (6)

and

for $La_{0.5}Sr_{0.5}Fe^{+3}_{0.8}Fe^{+4}_{0.2}O_{2.7}Cl_{0.3}$: $t = 0.87$. (7)

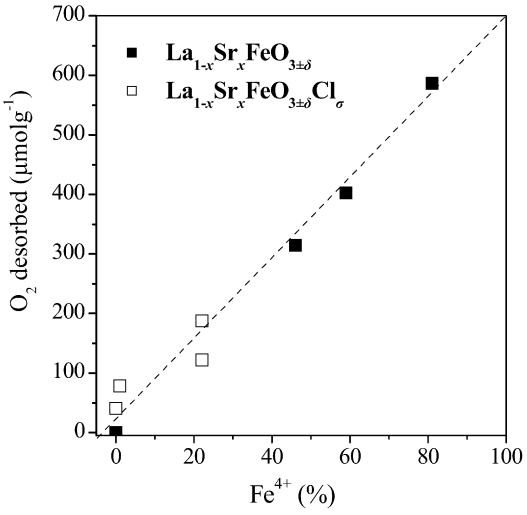

Fig. 4. The amount of desorbed oxygen in μmol g^{-1} s^{-1} versus the % amount of Fe^{4+} in all tested samples.

We can see that the substitution of oxygen by chlorine resulted in a decrease in t values, whereas the substitution of La by Sr led to an increase in t values. Now for $0.75 < t < 0.90$, the stabilized structures were orthorhombic, whereas for $0.90 < t < 1.00$, they were rhombohedral [27]. Thus, it seems that the addition of Cl maintained the values of $t < 0.90$ and favored formation of a well-organized orthorhombic structure. In addition, the addition of Cl somehow counterbalanced the action of Sr, the addition of which worked toward increasing the t values even above 0.90 and thus destabilizing the orthorhombic structure toward a rhombohedral one. The foregoing might be at least one of the reasons, among others, for the stabilization of various crystal phases and destabilization of others in the system La–Sr–Fe–O–Cl.

Finally, the loss of O_2 in the TPD experiments corresponds exactly to the stoichiometry

$$4SrFe^{4+}O_3 \leftrightarrow (1/2)O_2 + 3SrFe^{4+}O_3/SrFe^{3+}O_{2.5} \quad (8)$$

or

$$Sr_4Fe_4^{4+}O_{12} \leftrightarrow (1/2)O_2 + Sr_4Fe_3^{4+}Fe^{3+}O_{11.5}. \quad (9)$$

According to Wilson and Predith [28] the creation of oxygen vacancies results in a slight deformation of the lattice (as shown in Fig. 5), whereas the Fe ion in the center of the octahedron relaxes toward the opposite direction from the vacancy without destroying the structure. When oxygen is introduced back into the system, the solid obtains the original structure. Certainly, similar effects can be seen here, and this facile flip-flop of oxygen influences the catalytic properties of the solids, as will be discussed next.

3.4. Catalytic activity versus the degree of substitution

A comparison of the reaction rates (μmol g^{-1} s^{-1}) of CH_4 oxidation on the $La_{1-x}Sr_xFeO_{3\pm\delta}$ and $La_{1-x}Sr_xFeO_{3\pm\delta}Cl_\sigma$ catalysts at three typical temperatures (480, 560, and 640 °C), as a function of x, is presented in Fig. 6. Figs. 6a and 6b plot the

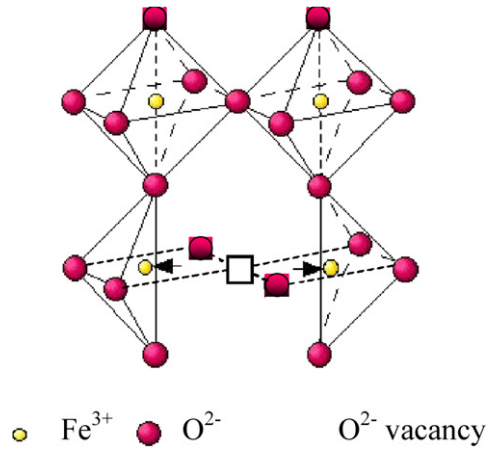

Fig. 5. Schematic illustration of the reaction (9) representing the loss of one oxygen atom from a perovskite unit cell $Sr_4Fe_4O_{12}$.

calculated reaction rate R_{CH_4} values for the products of reaction $CH_4 + O_2$, whereas Figs. 6c and 6d show the corresponding plots for the products of reaction $CH_4 + N_2O$. The reaction rates are expressed per unit mass, because the specific surface areas of the tested solids were found to be <4 m^2 g^{-1}, and such values contain large relative errors. We can see that the samples of the first, oxidic group (left part of Fig. 6) exhibit obviously higher catalytic activity compared with those of the second, chlorinated group (right part) at all temperatures. We also observe that the R_{CH_4} values were considerably lower when N_2O was used as the oxidant than when oxygen was used as the oxidant (Figs. 6c and 6d). These values decreased more abruptly as the degree of substitution x increased, whereas in the reactions with oxygen (Figs. 6a and 6b), the decrement was gradual. Especially at low temperatures (480 and 560 °C), the preponderance of the reaction using oxygen over that using N_2O is clear. Fig. 6 gives plots of the quantity of desorbed O_2 in μmol per g of solid (from O_2-TPD experiments) versus x (Sr content), to show the opposite behavior characterizing the graphs of $R_{CH_4} = f(x)$ and desorbed $O_2 = f(x)$.

It is well established that substitution of the trivalent A-site metal ion (La) with a divalent metal cation (Sr) in perovskite oxides leads to the modification of the oxidation state of the B cation. This is accompanied by the formation of structural defects, resulting in the establishment of nonstoichiometry. For perovskites based on Mn, the above substitution results in the creation of oxygen excess, whereas for perovskites based on Co, it leads to the creation of oxygen defects. The Fe-containing perovskites show an intermediate behavior [29,30]. These observations have been confirmed by our data, showing that substitution of La by Sr led to a higher oxidation state for Fe, so that the samples with the maximum Sr content ($x = 0.8$) had the highest percentage of Fe^{4+}.

As shown in Fig. 6, catalytic activity for both reactions and both groups of samples declined as the degree of Sr substitution increased. The drop in catalytic activity was more obvious for the products of reaction $CH_4 + N_2O$. In particular, the activity for the substituted chlorinated samples became negligible. An explanation for the results obtained for this reaction is perhaps that the oxygen species generated from the decom-

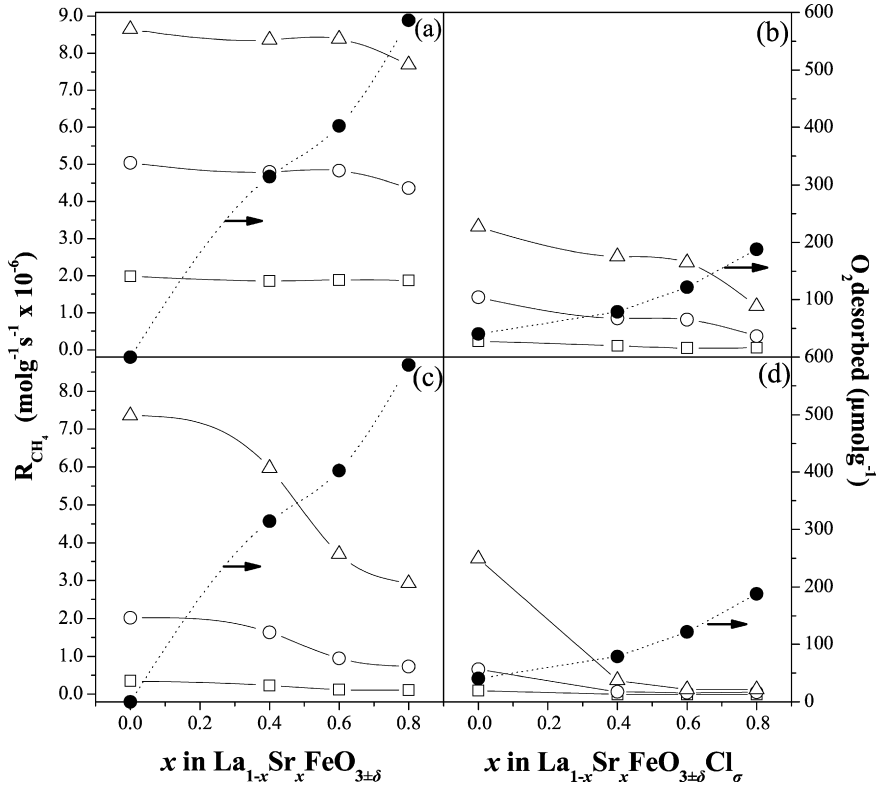

Fig. 6. Intrinsic activity (μmoles of CH_4 converted per gram of catalyst and per sec) of the samples for three typical temperatures 480 (square), 560 (circle), and 640 °C (triangle) (left axis) and the fluctuation of the amount of desorbed oxygen (right axis), versus the degree of substitution x for the samples tested in reaction with O_2 (a, b) and for the samples tested in reaction with N_2O (c, d).

position of N_2O were strongly adsorbed, covered the oxygen deficiencies on the surface, and poisoned the catalyst surface, as chlorine does. On the other hand, according to our TPD experiments, desorption of adsorbed gas oxygen occurred mainly at 350–400 °C. Therefore, in the temperature range at which the catalytic experiments were carried out (400–800 °C), gas oxygen was not strongly adsorbed and thus did not poison the surface. Therefore, higher activities were reached for the products of reaction $CH_4 + O_2$ over the corresponding samples. At low temperatures, methane combustion is a suprafacial reaction involving oxygen from the gas phase [31]. Combustion is suppressed, because the required amount of oxygen is strongly bounded on the surface of the solid. In contrast, at higher temperatures, methane reacts with the oxygen from the catalyst bulk via an intrafacial mechanism [31]. Therefore, at high temperatures, the conversion of CH_4 on substituted catalysts is comparable with that on unsubstituted samples (Fig. 6).

Desorption of oxygen during TPD experiments from such solids is usually attributed to oxygen species situated at structural defects and/or oxygen from the bulk of the solid [32,33]. These two types of oxygen are known in the literature as α-oxygen (desorbed at 300–500 °C), corresponding to surface-desorbed oxygen originating in the reduction process involving the B-site metal and the formation of anionic vacancies and β-oxygen (desorbed at 600–800 °C), which is assigned to tightly bonded lattice oxygen [34].

As mentioned earlier (see Figs. 3c and 3d), the $La_{1-x}Sr_xFeO_{3\pm\delta}$ samples desorbed oxygen mainly at low temperature, with only small amounts desorbed above 600 °C. The corresponding desorption on the $La_{1-x}Sr_xFeO_{3\pm\delta}Cl_\sigma$ samples occurred at high temperature only (β-oxygen), whereas the generation of α-oxygen was limited. But on the $La_{1-x}Sr_xFeO_{3\pm\delta}$ samples, oxygen vacancies, generated from the insertion of Sr into the lattice and leading to high values of Fe^{4+}, were occupied by α-oxygen. This type of oxygen is considered more active [35] and reacts with methane at a lower temperature compared with β-oxygen, resulting in higher activity for the $La_{1-x}Sr_xFeO_{3\pm\delta}$ samples.

Table 4 compares the catalytic performance of the tested samples with similar systems from the literature. Such a comparison is made only for reaction I, because no data were found for reaction II using perovskite systems. The parameter used for the comparison was $T_{50\%}$, the temperature at which 50% of the combustion was completed. We find that the activity of our samples is comparable with that of similar perovskite systems and with the 0.38% Pt/Al_2O_3 catalyst.

3.5. Deactivation role of chlorine

A quantitative way to describe the poisoning effect of Cl on the catalytic activity can be based on the standard kinetics of deactivation [33,34] expressed by the equation

$$-\mathrm{d}A/\mathrm{d}C_{\mathrm{Cl}} = kC_{\mathrm{Cl}}^n, \tag{10}$$

where $A = R/R_o$, with R and R_o the poisoned and unpoisoned reaction rates, in our case $A = R_{\mathrm{Cl}}/R_{\mathrm{ox}}$; R_{Cl} and R_{ox} are the

Table 4
Comparison of catalytic activity with similar systems from literature

Catalyst	Experimental conditions	$T_{50\%}$ (°C)	Ref.
	Reaction $CH_4 + O_2$		
$LaMnO_3$	2% CH_4 in air flow sv = 45000–50000 h^{-1}	579	[36]
$LaMnO_3$	0.4% CH_4, 10% O_2 in N_2 sv = 40000 h^{-1}	510	[37]
$SrFeO_{2.74}$	N_2:CH_4:O_2 = 4:2:1 Q = 130 ml/min, $W/F_{CH_4} = 2$	677	[38]
$LaMnO_3$	1.5% CH_4, 18% O_2 in He Q = 1.2 ml/s	540	[39]
$LaMn_{0.5}Mg_{0.5}O_3$	1.5% CH_4, 18% O_2 in He Q = 1.2 ml/s	490	[39]
$LaMnO_3$	0.5% CH_4, 10% air flow in N_2 Q = 40 N cm^3/min	440	[40]
$La_{0.8}Sr_{0.2}MnO_3$	3.5% CH_4, 17% O_2 in N_2 sv = 20000 ml/g_{cat} h	585	[41]
$La_{0.8}Sr_{0.2}FeO_{3-\delta}$	2.0% CH_4, 98.0% air flow Q = 100 ml/min	600	[42]
0.38% Pt–Al_2O_3	2% CH_4, 10% O_2 in N_2 W/F = 21.99 g h mol^{-1}	522	[43]
$La_{0.7}Sr_{0.3}FeO_3$	4.35% CH_4, 8.7% O_2 in He Q = 115 ml/min	580	This work
$La_{0.8}Sr_{0.2}FeO_{3\pm\delta}Cl_\sigma$	4.35% CH_4, 8.7% O_2 in He Q = 115 ml/min	700	This work
	Reaction $CH_4 + N_2O$		
$LaFeO_3$	5.0% CH_4, 20.0% N_2O in He Q = 120 ml/min	620	This work
$La_{0.8}Sr_{0.2}FeO_{3\pm\delta}Cl_\sigma$	5.0% CH_4, 20.0% N_2O in He Q = 120 ml/min	730	This work

reaction rates over the chlorinated and oxidic catalysts; C_{Cl} is the concentration of poison (chlorine) in the catalyst; n is the order of deactivation; and k is a constant value. The parameters n and k are to be determined. After separating variables and integration in the limits 1 to A for A and 0 to C for C, we obtain

$$A = 1 - \frac{k}{n+1}C^{n+1} = \frac{R_{Cl}}{R_{ox}}, \tag{11}$$

and then

$$\log\left[1 - \frac{R_{Cl}}{R_{ox}}\right] = \log\left(\frac{k}{n+1}\right) + (n+1)\log C_{Cl}. \tag{12}$$

Then from plots of the left side term versus $\log C_{Cl}$, we can estimate the slope $(n+1)$ and the intercept $k/(n+1)$, from which the values of n and k can be easily determined. We successfully applied this procedure for the reaction

$$CH_4 + 2O_2 \rightarrow CO_2 + 2H_2O$$

for the four pairs of oxidic–chlorinated solids specified in Table 2 at various reaction temperatures (560, 600, 640, 680, and 720 °C). Table 5 gives the results for the values of n, the main parameter of deactivation, and k, whereas Fig. 7 provides verification of those results in plots of $(R_{Cl}/R_{ox}) = f(C_{Cl}^{n+1})$.

From Fig. 7, we observe that the intercept was indeed close to unity, as expected according to (11). The order of deactivation n varied from $n = -0.91$ at 560 °C to -0.63 at 720 °C in a regular way, and the value of the constant k also was affected by temperature via an Arrhenius-type relationship, $k = A\exp(-E/\text{room temperature})$, where E is the activation energy of deactivation, to be determined. Considering this, plots of $\ln k$ versus $1000/T$ provide an energy of deactivation of about 43–44 kJ mol^{-1}.

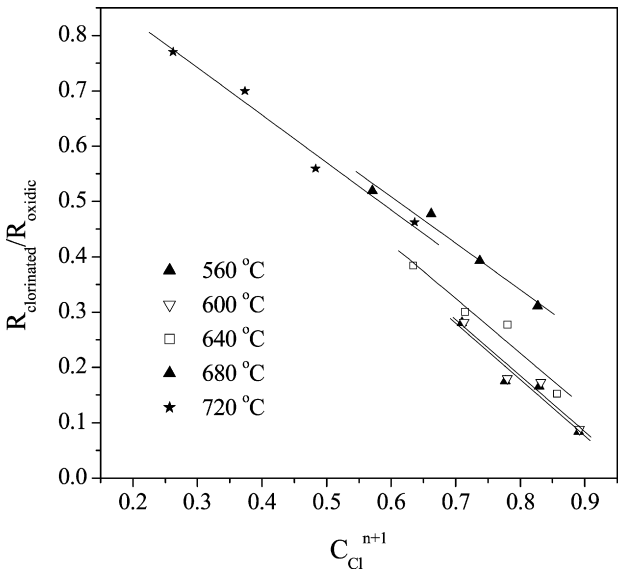

Fig. 7. Deactivation plots of the ratio R_{Cl}/R_{ox} vs C_{Cl}^{n+1} for the product of reaction $CH_4 + O_2$ at various reaction temperatures.

Table 5
Deactivation parameters k and n for the reaction $CH_4 + 2O_2 \rightarrow CO_2 + 2H_2O$ at various reaction temperatures

Reaction temperature (°C)	n	k
560	−0.91	0.10
600	−0.91	0.09
640	−0.88	0.12
680	−0.85	0.13
720	−0.63	0.31

In the case of reaction

$$CH_4 + 4N_2O \rightarrow CO_2 + 2H_2O + 4N_2,$$

a treatment like the above was not possible. This may be because the oxygen generated from the N_2O decomposition is strongly adsorbed as well and poisons the surface, as chlorine does. The process of deactivation is complex and cannot be quantified.

4. Conclusion

A comparison of the structure and solid-state composition of substituted perovskite-type solids of oxidic ($La_{1-x}Sr_xFeO_{3\pm\delta}$) and chlorinated ($La_{1-x}Sr_xFeO_{3\pm\delta}Cl_\sigma$) forms showed that the gradual substitution of La^{3+} by Sr^{2+} resulted in an increased Fe^{4+}/Fe^{3+} ratio in both groups of solids. The substitution also affects linearly the amount of desorbed oxygen. It was found that the chlorinated solids contain less Fe^{4+} and desorb less oxygen compared with the corresponding oxidic solids.

The study of the methane oxidation by oxygen and nitrous oxide over $La_{1-x}Sr_xFeO_{3\pm\delta}$ and $La_{1-x}Sr_xFeO_{3\pm\delta}Cl_\sigma$ catalysts showed that the first group was more active. In addition,

the samples with low Sr content were more active compared with those with higher Sr content. The decreased activity in both groups of solids was related to the increased amount of desorbed oxygen as well as the increased Fe^{4+} content in the solids.

The lower activity of the chlorinated samples was attributed to a poisoning effect by the chlorine, which was quantified using proper deactivation kinetics. Especially for the oxidation with oxygen, the reaction rate was found to decrease linearly with the amount of chlorine in the sample.

Acknowledgments

Part of this work was carried out with financial support from the project "Human Networks of Scientific and Technological Training" of the General Secretariat for Research and Technology. Financial support was also provided by the HERAKLEITOS and PYTHAGORAS programs from the Greek Ministry of Education. The authors thank the Ring of the Laboratory Units and Centers of the University of Ioannina for the XRD, TG experiments, and SEM-EDS analysis.

References

[1] N. Mizuno, M. Tanaka, M. Misono, J. Chem. Soc. Faraday Trans. 88 (1992) 91.
[2] L. Simonot, F. Garin, G. Maire, Appl. Catal. B Environ. 11 (1997) 181.
[3] V.C. Belessi, P.N. Trikalitis, A.K. Ladavos, T.V. Bakas, P.J. Pomonis, Appl. Catal. A Gen. 177 (1999) 53.
[4] L. Fabbrini, I. Rossetti, L. Forni, Appl. Catal. B Environ. 63 (2006) 131.
[5] S. Cimino, G. Landi, L. Lisi, G. Russo, Catal. Today 117 (2006) 454.
[6] C. Mure, P. Duran, in: L.G. Tejuca, J.L.G. Fierro (Eds.), Properties and Applications of Perovskite-Type Oxides, Marcel Dekker, New York, 1993.
[7] J.B. Yang, X.D. Zhou, Z. Chu, W.M. Hikal, Q. Cai, J.C. Ho, D.C. Kundaliya, W.B. Yelon, W.J. James, H.U. Anderson, H.H. Hamdeh, S.K. Malik, J. Phys. Condens. Matter 15 (29) (2003) 5093.
[8] S.E. Dann, D.B. Curie, M.T. Weller, M.F. Thomas, A.D. Al-Rawwas, J. Solid State Chem. 109 (1994) 134.
[9] V.C. Belessi, C.N. Costa, T.V. Bakas, T. Anastasiadou, P.J. Pomonis, A.M. Efstathiou, Catal. Today 59 (2000) 347.
[10] K.S. Roh, K.H. Ryu, C.H. Yo, J. Mater. Sci. 30 (5) (1995) 1245.
[11] H. Falcon, M.J. Martinez-Lope, J.A. Alonso, J.L.G. Fierro, Solid State Ionics 131 (3–4) (2000) 237.
[12] K. Nomura, Z. Homonnay, A. Vertes, V. Chechersky, A. Nath, Y. Ujihira, T. Hayakawa, K. Takehira, Czech. J. Phys. 47 (5) (1997) 517.
[13] H.X. Dai, C.F. Ng, C.T. Au, Catal. Lett. 57 (1999) 115.
[14] Y. Guo, X. Zhang, R. Wäppling, J. Alloys Compd. 306 (2000) 133.
[15] S.J. Conway, J.H. Lunsford, J. Catal. 131 (1991) 513.
[16] I. Lee, K.Y.S. Ng, Catal. Lett. 2 (1989) 403.
[17] H.X. Dai, C.F. Ng, C.T. Au, J. Catal. 189 (2000) 52.
[18] H. Yamamoto, H.Y. Chu, M. Xu, C. Shi, J.H. Lunsford, J. Catal. 142 (1993) 325.
[19] E.N. Voskresenskaya, L.I. Kurteeva, G.G. Pervyshina, A.G. Anshits, Catal. Today 24 (1995) 277.
[20] H.N. Kong, Y. Kimochi, M. Mizuochi, R. Inamori, Y. Inamori, Sci. Total Environ. 290 (2002) 59.
[21] S. Sugiyama, K. Abe, H. Hayashi, Y. Matsumura, J. Moffat, J. Mol. Catal. A Chem. 144 (1999) 347.
[22] A.A. Leontiou, A.K. Ladavos, T.V. Bakas, T.C. Vaimakis, P.J. Pomonis, Appl. Catal. A Gen. 241 (2003) 143.
[23] N.N. Greenwood, T.C. Gibb, Mössbauer Spectroscopy, Chapman and Hall, London, 1971, p. 46.
[24] G. Longworth, G.J. Long (Eds.), Mössbauer Spectroscopy Applied to Inorganic Chemistry, vol. 1, Plenum Press, New York, 1984, p. 43.
[25] V.M. Goldschmidt, Skr. Nor. Viedenk.-Akad. Kl. I: Mater.-Naturvidensk. Kl. 8 (1926).
[26] D.R. Lide, Handbook of Chemistry and Physics, 84th ed., CRC Press.
[27] F.S. Galasso, Structure Properties and Preparation of Perovskite-Type Compounds, Pergamon Press, Oxford, 1969.
[28] A. Wilson, A. Predith, Simulation of oxygen ion ordering as a result of temperature change, Spring 2002, http://beowulf.lcs.mit.edu/18.337-2002/projects-2002/a_wilson/18.337/proposal.ps.
[29] L.G. Tejuca, J.L.G. Fierro, J.M.D. Tascon, Adv. Catal. 36 (1989) 237.
[30] Y. Wu, T. Yu, B.S. Dou, C.X. Wang, X.F. Xie, Z.L. Yu, S.R. Fan, Z.R. Fan, L.C. Wang, J. Catal. 120 (1989) 88.
[31] J.L.G. Fierro, Catal. Today 8 (1990) 153.
[32] N. Yamazoe, Y. Teraoka, T. Seiyama, Chem. Lett. (1981) 1767.
[33] D. Ferri, L. Forni, Appl. Catal. B Environ. 16 (1998) 119.
[34] T. Seiyama, Catal. Rev.-Sci. Eng. 34 (1992) 281.
[35] J.G. McCarty, H. Wise, Catal. Today 8 (1990) 231.
[36] H. Arai, T. Yamada, K. Eguchi, T. Seiyama, Appl. Catal. 26 (1986) 265.
[37] P. Ciambelli, S. Cimino, S. De Rossi, M. Faticanti, L. Lisi, G. Minelli, I. Pettiti, P. Porta, G. Russo, M. Turco, Appl. Catal. B 24 (2000) 243.
[38] H. Falcon, J.A. Barbero, J.A. Alonso, M.J. Martinez-Lope, J.L.G. Fierro, Chem. Mater. 14 (2002) 2325.
[39] G. Saracco, F. Geobaldo, G. Baldi, Appl. Catal. B 20 (1999) 277.
[40] L. Marchetti, L. Forni, Appl. Catal. B 15 (1998) 179.
[41] Y. Liu, H. Zheng, J. Liu, T. Zhang, Chem. Eng. J. 3995 (2002) 1.
[42] R. Doshi, C.B. Alcock, N. Gunasekaran, J.J. Carberry, J. Catal. 140 (1993) 557.
[43] T.F. Garetto, C.R. Apesteguía, Catal. Today 62 (2000) 189.